X 5 Quantum Computing with Semiconductor Quantum Dots

Carola Meyer
Institut für Festkörperforschung (IFF-9)
Forschungszentrum Jülich GmbH

Contents

1 Introduction

Quantum dots can be used to confine single electrons as discussed by M. Wegewijs in the lecture "Spin and Transport in Quantum Dots". The quantum computing concepts based on quantum dots can be subdivided in two main branches: optical concepts and electrical concepts. In most of the optical concepts, the two level system representing the quantum bit (qubit) consists of exciton states. These are manipulated using polarized light. In electrical concepts, the spin states of electrons are used as qubit and manipulation can be done all-electrically.
This contribution will concentrate on spin states of electrons for quantum information focusing on the most important electrical concept known as "Loss-DiVincenzo proposal" [1]. It has been shown experimentally for this proposal that all of the "DiVincenzo criteria" (for a general introduction into Quantum Computing see lecture "Fundamental Concepts of Quantum Information Processing" by T. Schäpers) can be met as we shall see in the following.

2 The "Loss-DiVincenzo" proposal

A few years after the first implementation of the CNOT quantum gate using hyperfine and vibrational states of a $^9Be^+$ ion in an ion trap as qubits [2], a row of proposals for a solid state quantum computer appeared, based on cooper pairs [3], nuclear spins in silicon [4], and last but not least electron spins in GaAs quantum dots [1]. Daniel Loss and David DiVincenzo proposed a quantum computer based upon existing semiconductor technology.

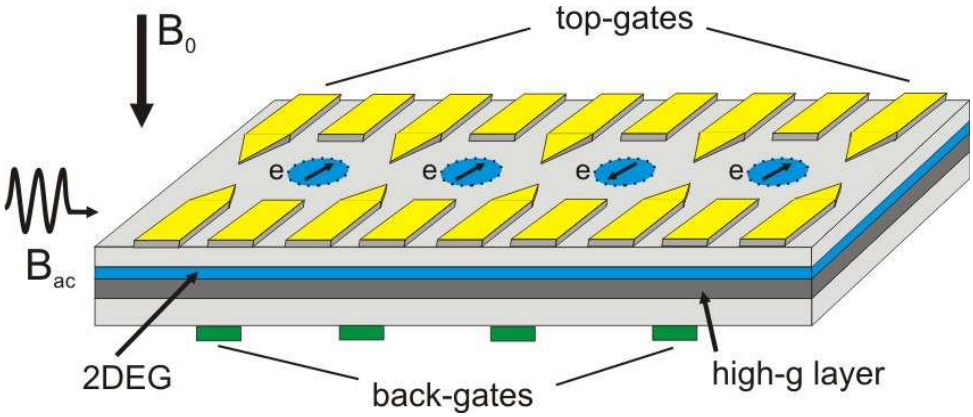

Fig. 1: *Scheme of the Loss-DiVincenzo proposal.The top gates are used to form quantum dots as well as to tune the interaction between them. An AC magnetic field is used to manipulate the electron spins. Back gates can draw the electrons into a layer with different g-factor, thus changing their resonance frequency.*

The scheme of this proposal is depicted in Figure 1. A two dimensional electron gas (2DEG) is formed by a GaAs/GaAlAs heterostructure. Voltages applied to electric top-gates are used to deplete certain regions of the 2DEG in such a way that a quantum dot with only a single electron inside remains. In a magnetic field $\boldsymbol{B_0} = (0, 0, B_z)$ the otherwise degenerate Zeeman states $|\uparrow\rangle$, $|\downarrow\rangle$ split up with energy difference $E_{Zee} = g\mu_B\hbar B_0$, with Landé factor $g = -0.44$ for GaAs and μ_B the Bohr magneton, and form the two level system used as a qubit. Initialization can be achieved by allowing the electron spins to reach their thermodynamic ground state at low temperature T, with $|E_{Zee}| \gg k_BT$ (with Boltzmann constant k_B). However, this is a very slow

process, because the relaxation rate from an exited spin state to the ground state has to be small in order not to loose the information of the qubit. We will see later that also a scheme for fast initialization exists.
The qubit states can be manipulated with an ac magnetic field applied perpendicular to B_0 just as in electron spin resonance (ESR). This ac magnetic field can be generated by passing an ac current through a wire close to the quantum dots. In order to be able to carry out single qubit rotations, the resonance frequency of the manipulated spin needs to differ from the resonance frequency of the spins in the other quantum dots. This can be achieved by a B_0 gradient along the chain of quantum dots or by g factor engineering. For the latter, the electron is pulled into a layer with a high g-factor by applying a voltage on a local back-gate. Thus, the energy splitting between the spin states and therefore the resonance condition is changed.
The Hamiltonian used for gate operations in a system with N qubits is

$$H(t) = \sum_{i}^{N} g_i(t) B_i(t) S_i + \sum_{i<j}^{N} J_{ij}(t) S_i(t) S_j, \tag{1}$$

with qubit sites i, j. The first term describes the single qubit gates as discussed above with $B(t) = B_0(t) + B_{ac}$. The second term describes two qubit gates, with the exchange interaction J_{ij} used for the qubit coupling. Only adjacent qubits need to be coupled, since information can be passed through the qubit chain with the SWAP gate. The coupling between two neighboring qubits, i.e. the potential barrier between two adjacent quantum dots, can be controlled by voltages applied to the top-gates. Therefore, the "Loss-DiVincenzo" proposal is in principle scalable. Since GaAs quantum dots have been extensively studied and the spins can be initialized in their ground state, the first two DiVincenzo criteria are fulfilled. In this lecture we will see that the other criteria, namely the qubit read-out, a universal set of quantum gates and long decoherence times are met as well.

3 Read-out of a single electron spin

In this section we will see how the electron spin state in a quantum dot can be measured. Two read-out schemes exist, one for a single quantum dot with $|\uparrow\rangle$, $|\downarrow\rangle$ as qubit states, and one with the singlet $|S\rangle$ and the triplet $|T_0\rangle$ state of a *two-electron* quantum dot as qubit. Both schemes have in common that the spin state is first converted into a charge state, which is then detected by the current through an adjacent quantum point contact (QPC). In this way, the measurement is decoupled from the qubit system and the back action of the read-out on the qubit state is minimized.
Before we look at the two schemes in more detail, we will briefly discuss the QPC detection. A QPC is a one-dimensional constriction in the 2DEG formed by top-gates (see inset Fig.2). Top-gate voltages or other potentials close by define how many electrons can pass the constriction at the same time, i.e. the number of available transport channels.
The conductance of a QPC shows a step-like behavior depending on the voltage applied to the top-gates as shown in Fig.2. Transport channels are opened one by one, while the applied gate voltage becomes more positive. Without external magnetic field the step hight is $2e^2/h$, since the two spin states of an electron are degenerate. If this degeneracy is lifted by applying an external magnetic field, additional steps appear at multiples of e^2/h [5].
In close proximity to a quantum dot, a QPC can be used as noninvasive voltage probe [6] that detects the number of electrons on the quantum dot. The QPC is operated in the middle between

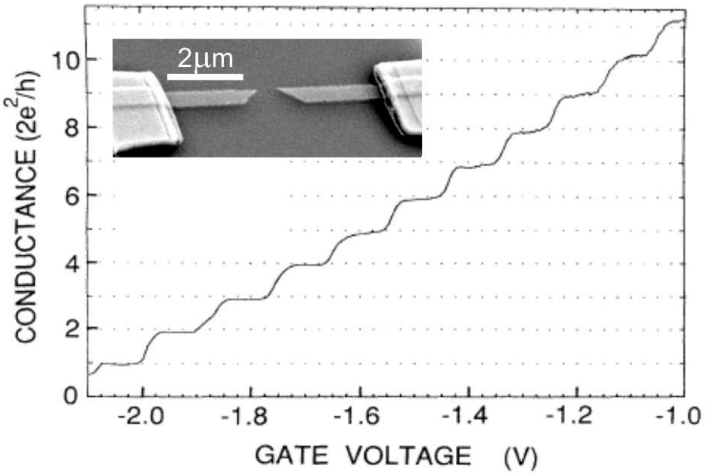

Fig. 2: *Stepwise increase of the QPC conductance at T = 0.6 K with changing top-gate voltage (from reference [5]). Inset: An example for a quantum point contact structure (adapted from http://pages.unibas.ch/phys-meso/Pictures/pictures.html).*

two current plateaus in order to obtain maximum sensitivity towards adding an electron to the quantum dot or removing it. Today this technique has been extended on double quantum dots measuring small signals of photon-assisted tunneling [7] and spin blockade [8].

3.1 Single shot read-out

In order to demonstrate the single shot read-out of a single electron spin, a quantum dot with a QPC next to it was fabricated as shown in Fig.3a. It is important that the gate R is closed completely, so that the current to the drain of the QPC is not influenced by a current through the dot. The QPC is adjusted to its working point with the gate Q. Tunneling events occur between the reservoir and the dot with rate Γ depending on the tunneling barrier influenced by gate L.

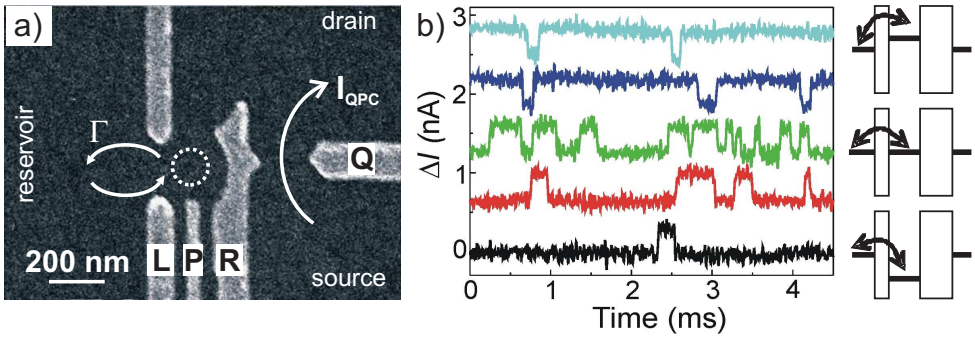

Fig. 3: *(a) Gate structure for a single quantum dot formed by gates R and L with adjacent QPC between Q and R. The potential barrier on the right is very high and tunneling between the dot and the reservoir occurs through the left barrier with rate Γ. (b) Tunneling events of a quantum dot measured trough the current of a QPC for different potentials on P. The dot is empty (high current) most of the time for the top trace while it is occupied (low current) most of the time for the bottom trace. When the electrochemical potential of the dot is aligned with the Fermi level of the reservoir, the electron tunnels back an forth. All images adapted from ref. [9].*

Since the read-out of a spin state is done via charge detection, we should first know how fast the charge state can be measured. This has been shown in ref. [9]. There, the quantum dot is set near to its $N = 0$ to $N = 1$ transition using gate P to tune the dot potential. The electron can then spontaneously tunnel back and forth between the dot and the reservoir, and the QPC current should exhibit a random telegraph signal (RTS) as shown in Fig.3b. The time the electron spends in the dot, i.e. when ΔI_{QPC} is in the low state, strongly depends on the position of the dot potential relative to the Fermi level of the leads. The current through the QPC was $I_{QPC} \approx 30$ nA with a bias voltage of $V_{bias} = 1$ mV, in agreement with the conductance of the QPC at its working point $G_{QPC} = e^2/h \approx (30\text{k}\Omega)^{-1}$. The shortest steps that clearly reached above the noise level were about 8μs long. Tunnel events occuring on a shorter timescale will be lost in the current noise of the QPC. Therefore, the spin-energy relaxation time T_1, i.e. the time after which a spin has flipped from its exited $|\downarrow\rangle$ state back to the ground state $|\uparrow\rangle$, of the spin in the quantum dot has to be much longer than 8μs. Otherwise the information stored in the qubit would be lost before it was even measured.
The single-spin-single-shot read-out was first demonstrated in the group of L. Kouwenhoven at TU Delft [10]. To detect the spin state of an electron, first a magnetic field B_0 has to be applied so that the degeneracy of the Zeeman states is lifted. In order to tune the dot potential quickly, voltage pulses with lengths of a few 100 ns are applied to gate P (Fig.3a). Figure 4 shows the pulse scheme used for the single spin read-out as well as the response of the QPC.

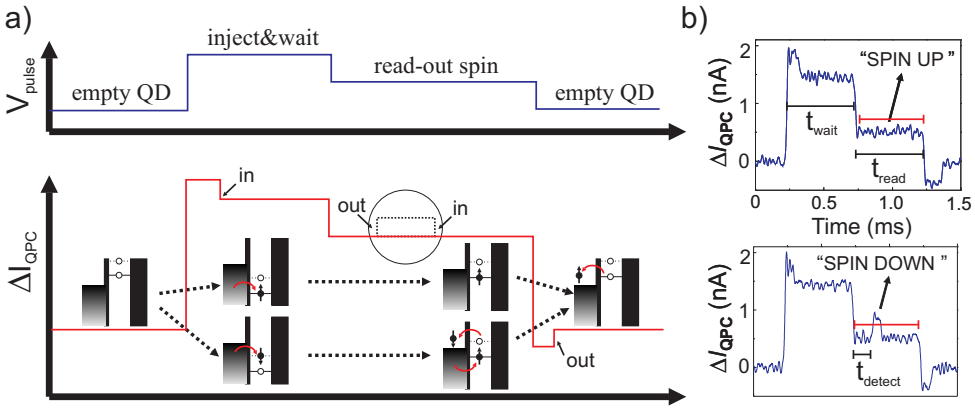

Fig. 4: *(a) Scheme of the single shot read-out. On the top the voltage levels applied as pulses on gate P (Fig.3a) are shown. The difference in the QPC current during the different stages is shown on the bottom along with the tunnel events. The signal during the read-out depends on the spin state (circle). In the case of "spin down", to additional tunnel events take place and the signal follow the dotted line. (b) Single shot measurements of a spin state. The top graph shows the trace of the QPC current for the "spin up" situation, where no tunneling events are measured during the read-out time t_{read}. On the bottom, the "spin down" case is depicted. During t_{read}, the threshold value of the QPC current (red line) is crossed indicating two additional tunneling events. The time t_{detect} is the time it takes for a "spin down" electron to tunnel out of the dot and thus related to the rate $\Gamma_\downarrow$ All figures adapted from [10].*

At the beginning the quantum dot potential is set to a low value, so that any remaining electron is pushed out of the dot. Then, a positive voltage pulse is applied to put both spin states below the Fermi level of the lead. The current of the QPC is changing as well, since it couples capacitively to the gate P as well. As soon as either a spin-up or a spin-down electron from the reservoir tunnels into the dot, the current of the QPC drops due the extra charge in the vicinity. The time

one has to wait for an electron to enter is directly connected to the tunneling rate $\Gamma = \Gamma_\downarrow + \Gamma_\uparrow$, which can be influenced by gate L (Fig.3b).
The spin to charge conversion is done in the third part of the pulse pattern. The potential of the dot is changed such that the spin-up ground state remains below the Fermi level of the lead, while the excited spin-down state lies above it. No tunneling events will happen in the first case (see Fig.4b, top), because the dot is in coulomb blockade. However, in the latter case, first the spin-down electron will tunnel out before the ground state is filled again with a spin-up electron from the lead. Therefore, two tunneling events will occur during the read-out time t_{read} (Fig.4b, bottom). Before a new cycle can be started, the potential of the dot is tuned so that both spin states are above the Fermi level and held there until the spin-up electron now occupying the dot has tunneled out.
In order to measure the relaxation time T_1, the spin-down fraction is recorded for different waiting times t_{wait}. During this time, a spin-down electron can relax to the ground state. The longer this time, the smaller the spin-down fraction will be, following an exponential decay as shown in Fig.5a. Fitting the data to $\alpha + C\exp(-t_{wait}/T_1)$ decay, a relaxation time of $T_1 \approx 0.55$ ms is obtained at $B_0 = 10$ T. This is almost two orders of magnitude longer than the time needed for the fast detection and the response of the QPC is thus quick enough.
Nevertheless, there is a finite probability α that a signal is measured during t_{read} although a spin-up electron was in the dot, for instance due to thermally activated tunneling or electrical noise (”dark counts”). This probability can be extracted directly from the T_1 measurement. It is simply the saturation value of the exponential decay. Unfortunately, a similar evaluation is not possible for the opposite case that occurs with probability β; the QPC current stays below the threshold although a spin-down electron was in the dot. The correlation between these probabilities is shown in the inset of Fig.5a.

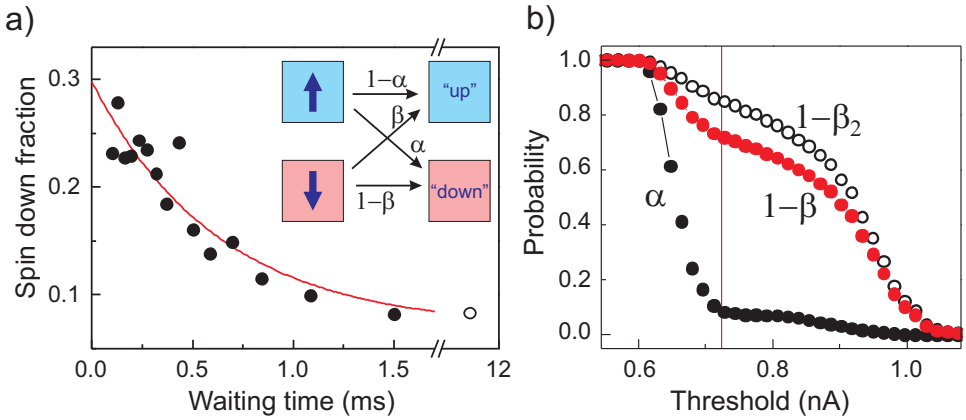

Fig. 5: *(a) T_1 relaxation measured with the single shot read-out. The probabilities for measuring a spin-up as a spin-down and vice versa are depicted in the inset. (b) Their values depend on the threshold set in the measurement (see Fig.4). The vertical red line marks the threshold value with the highest visibility. Adapted from [10].*

Two processes contribute to β which can be analyzed separately. First, a spin-down electron can relax to the spin-up state before the electron tunnels out with probability $\beta_1 = 1/(1 + T_1\Gamma_\downarrow)$. $\Gamma_\downarrow$ can be obtained from a histogram of the detection time t_{detect} (see Fig.4b for definition). In ref. [10] its value was found to be $\Gamma_\downarrow^{-1} \approx 0.11$ ms yielding $\beta_1 \approx 0.17$. Second, if the spin-down electron is replaced within 8μs with a spin-up electron the resulting QPC step may be too small to detect. The probability β_2 of this event depends on the value of the threshold

(red line in Fig.4b). It can be measured reversing the pulse sequence [10]. The empty levels are tuned to the read-out postition (4a). At the beginning of this pulse, a $|\uparrow\rangle$ should tunnel into the dot raising the QPC current above the threshold. The probability β_2 is obtained from the fraction of traces where this step is missed. The result is shown as $1-\beta_2$ in Fig.5 as well as the threshold dependence of α and $1-\beta$, the total spin-down fidelity is given by $1-\beta \approx (1-\beta_1)(1-\beta_2)+(\alpha\beta_1)$.
The so-called visibility is a very important number for quantum computing, since it is a measure for the probability of a correct qubit measurement. For the single spin read-out discussed here, the visibility is

$$V = 1-\alpha-\beta. \tag{2}$$

The red line in Fig.5b marks the threshold value at which this expression has its maximum ($\alpha \approx 0.07$, $\beta_1 \approx 0.17$ and $\beta_2 \approx 0.15$). Therefore, the fidelity for the spin-down and the spin-up state is $(1-\beta) \sim 0.72$ and $(1-\alpha) \sim 0.93$, respectively [10]. The visibility of the single shot measurement, however, is only 65%, i.e. the chance to get a wrong result is 35%. Of course, this would be inacceptable for a computer, but for a proof of concept this is a good result, especially when compared to other implementations. Repeating the same calculation several times can already improve the accuracy. Lowering the electron temperature (smaller α) and a faster QPC measurement (smaller β) will increase the visibility as well.
However, this read-out method suffers from other disadvantages. It is very sensitive to fluctuations of the electrostatic potential, the Zeeman splitting has to be much larger than the thermal energy, and high frequency noise can spoil the read-out due to photon-assisted tunneling, i.e. when the ground state electron absorbs a microwave photon and gains enough energy to tunnel out of the dot into the reservoir.

3.2 Singlet-Triplet read-out

This method circumvents the problems of the single shot read-out described before and is described in ref. [11]. It discriminates between singlet $|S\rangle$ and triplet $|T\rangle$ states of a quantum dot and is therefore used as read-out for a *two-electron* quantum dot. Thus, the quantum dot is tuned near to its $N=1$ to $N=2$ transition. The device geometry is similar to the structure in Fig.3a.
The pulse sequence used for the read-out and relaxation time measurement is shown in Fig.6a. First, the dot potential is tuned, so that the $N=1$ to $N=2$ transition is above the Fermi level of the reservoir for both, the ground state $|S\rangle$ as well as the excited state $|T\rangle$. The quantum dot now contains one electron. Then, a pulse is applied and both states are pulled below the Fermi level. After some time, an electron tunnels into the dot with Γ_T for the triplet state and Γ_S for the singlet state. The electron tunnels out in the last step again with the rate corresponding to its state.
For the spin to charge conversion, which is implemented with this step, it is required that the tunneling rate of the triplet is much larger than the rate of the singlet ($\Gamma_T \gg \Gamma_S$). The tunneling of an electron from the singlet state with $\Gamma_S = 2.5$ kHz is slow enough to be measured. As long as the dot remains occupied with two electrons, the current of the QPC will be below the starting value. Only after one electron has left, the level will be at the value corresponding to $N=1$ electrons in the dot. The tunneling of the triplet state, however, happens too fast to be detected ($\Gamma_T \sim 100$ kHz) and the current of the QPC current reaches the original value right after the end of the voltage pulse. A low pass filter of 20 kHz added to the electronic measurement assures that the tunneling from the triplet state is not detected.

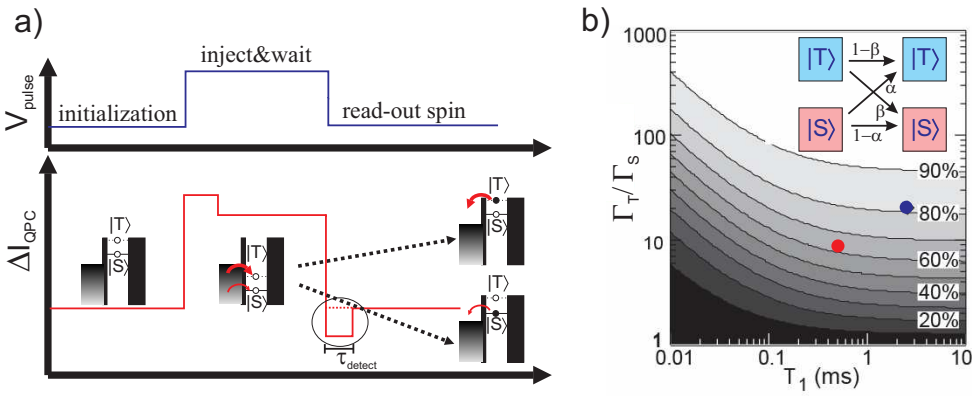

Fig. 6: *(a) Pulse sequence for the Singlet-Triplet read-out. The thicknes of an arrow depicts the tunnel rate. During the detection time τ_{detect} the QPC current drops only, if the state is a singlet. (b) Visibility depending on the ratio of the tunneling rates and the relaxation time for $\Gamma_S = 2.5$ kHz. Adapted from ref. [11].*

The visibility V as defined in equation (2) of this read-out depends on the tunneling rates Γ_T and Γ_S, the relaxation rate T_1, the time τ at which the number of electrons is measured. The probabilities α and β (for definition see Fig.6) are

$$\alpha = 1 - e^{-\Gamma_S \cdot \tau} \tag{3}$$

$$\beta = \frac{(1/T_1)e^{-\Gamma_S \cdot \tau} + (\Gamma_S - \Gamma_T)e^{-(\Gamma_S + 1/T_1)\cdot \tau}}{\Gamma_S + 1/T_1 - \Gamma_T}. \tag{4}$$

With (3) and (4) inserted in (2), the visibility depending on the ratio of the tunnel rates and the relaxation rate is shown in Fig.6b. For values of the visibility $V = 65\%$ and of the relaxation time $T_1 = 0.5$ ms as from the experiment in the previous section the ratio of the tunnel rates needed is $\Gamma_T/\Gamma_S = 10$ (marked by the red dot in Fig.6b).
The relaxation time can be obtained by measuring the triplet fraction for different waiting times as done in ref. [11]. The parameters α and β can be extracted from the same measurement (see Fig.7). The maximum visibility is 81% for optimized threshold ($\Delta I_{QPC} = -0.4$ nA) and time $\tau_{detect} = 70\mu$s (blue dot in Fig.6). The relaxation time obtained in this experiment was $T_1 = 2.58$ ms for $B = 0.02$ T. This is much longer than the relaxation time measured before at $B = 10$ T and a first indication that T_1 depends on the magnetic field, which we will discuss in more detail later.
The visibility reached with the read-out methods presented here might seem to be low. For a working quantum computer this is true, but still there are ways for improvement, e. g., lowering the electron temperature will reduce the "dark counts" α and a faster charge detection will reduce β [10]. A higher Γ_T/Γ_S ratio will yield a larger visibility for the singlet-triplet read-out. The visibility reached so far, however, is already sufficient for first demonstrations of qubit gates and for a proof of concept we can assume the read-out DiVincezo criterium to be fulfilled.

4 Manipulation of electron spins

After learning that gate pulses can be used to quickly tune the states of a quantum dot, it is easy to understand how a fast initialization can be done. A magnetic field is applied, so that the

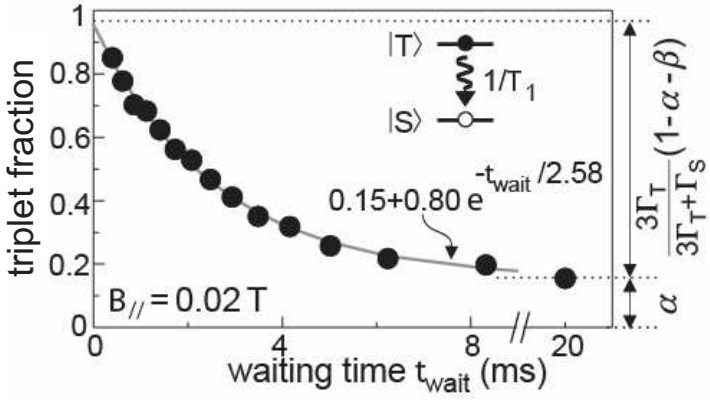

Fig. 7: *Measurement of the $|T\rangle \rightarrow |S\rangle$ relaxation time [11]. The probabilities α and β as defined in Fig.6b can be obtained as shown on the right.*

spin states are split by the Zeeman energy. First, both levels are pulsed above the Fermi level of the leads and the dot is emptied. Then, the levels are pulled down so that the spin-up level is below the Fermi level but the spin-down state is still above the Fermi level. After a time τ related to the tunneling rate, the spin-up level will be filled. The number of electrons in the dot is measured with a QPC. Now we know our initial state to be $|\uparrow\rangle$ and we can start to manipulate the spin state either by single qubit operations, i.e. single spin rotation using the first term of the Hamiltonian in equation (1), or by interaction between two qubits, using the exchange coupling J(t) of the second term, thus implementing a two-qubit gate like the $\sqrt{SWAP}$.

4.1 Single spin rotation

The state of an electron spin can be manipulated by electron spin resonance (ESR). If the spin is irradiated with an AC magnetic field B_1 with the same frequency as the Larmor frequency of the spin, i. e. the frequency of the Zeeman splitting, the spin will rotate. The angle of the rotation depends on the amplitude and duration of the B_1 pulse. This angle determines what kind of single spin gate is done, e.g., π (or 180°) corresponds to a spin-flip if the input was an eigenstate or, more generally speaking, it is a NOT gate. For more details about spin resonance, see the lecture "Donors for Quantum Information Processing" of M. Brandt or as an example for a textbook ref. [12].

In order to manipulate the electron spin in a quantum dot, an AC magnetic field of at least about 1 mT has to be coupled locally to the dot. This is much more easily said than done, since the electron temperature has to be kept very low ($\sim$ 100 mK) and high frequency irradiation always leads to dissipation of energy. The AC magnetic field is created by an AC current through a wire close to the quantum dot (see Fig.8a), with a dissipation of 10μW for $B_1 = 1$ mT and 250μW for $B_1 = 5$ mT, respectively. This requires a cooling power for the dilution refrigerator of about 300μW at 100 mK.

An ESR experiment could be done as follows. The spin is initialized in its ground state $|\uparrow\rangle$ in coulomb blockade while the level for the excited spin state $|\downarrow\rangle$ is split off by the Zeeman energy E_{Zee} and aligned between the Fermi levels of the leads (Fig.8b). In a second step, the AC magnetic field is applied, changing the spin state. Thus, the coulomb blockade is lifted and an additional current peak appears at higher gate voltage (Fig.8c,d). However, many other processes can lift the coulomb blockade as well. A current will flow independently of the ro-

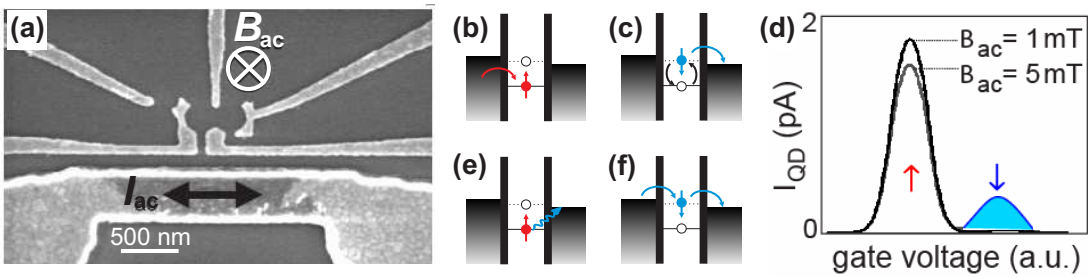

Fig. 8: *(a) Quantum dot structure with a strip line close by that creates an AC magnetic field. (b)-(d) Scheme for an ESR experiment. (e)-(f)The current due to ESR can be completely covered by photon-assisted tunneling.*

tation of the spin in the quantum dot, if the spins of the electrons in the leads have the same resonance frequency as the spin of the electron in the dot, or if heat dissipation smears out the state occupation at the Fermi level of the leads. Photon-assisted tunneling is another process that can totally mask the desired signal, which is due to ESR. In this process, the electron in coulomb blockade absorbs a photon and can tunnel directly to the drain (Fig.8e), thus lifting the coulomb blockade for transport through the excited spin state (Fig.8f). This is due to high frequency electric fields which cannot be totally suppressed. The influence of all these processes can be cancelled or at least reduced if both spin levels are pulled deep into the coulomb blockade regime by a voltage pulse. The Zeeman splitting has to be much smaller than the energy difference between the upper spin level and the Fermi level of the leads. The spin is manipulated and afterwards the electrochemical potential of the dot is pulsed back to its original position and the spin orientation is detected by either of the methods described in section 3.
The same concept can be used in a double quantum dot system with one electron in each dot (see Fig.9a). Since the exchange coupling J is very small in this configuration, the electrons can be treated as if they were separated. In this case, spin blockade as described in the lecture "Spins and Transport through quantum dots" by M. Wegewijs can be used for initialization and read-out of the system. The double dot is prepared in spin blockade, i.e. the spins in the two dots are parallel. Then, the electrochemical potential of the left dot is tuned to be deep below the transport window. An AC magnetic field rotates the spin and the electrochemical potential is raised to its former level. If the spin state has been rotated to form a singlet with the electron in the right dot, the spin blockade is lifted and a current flows. This sequence has to be repeated many times to get enough statistics. The Rabi oscillation of this experiment by Koppens et al. [13] is shown in Fig.9b. They could be observed up to pulse lengths of $1\,\mu$s, giving a lower bound for the decoherence time T_2 in this system.
One should note that the read-out scheme applied in this experiment is only sensitive to parity (parallel or antiparallel spin) and not a singlet-triplet read-out. Due to the nuclear field in GaAs, the triplet $|T_0\rangle$ and the singlet $|S\rangle$ are mixed and a $|T_0\rangle$ state will be transformed into $|S\rangle$ lifting the spin blockade. Without external magnetic field, $|T_+\rangle$ and $|T_-\rangle$ are also mixed, and no spin-blockade can be measured.

4.2 The $\sqrt{SWAP}$ operation

With regard to the requirement of a universal set of quantum gates for a quantum computer, we have seen that single qubit rotations can be done. In addition to the single spin rotations only the

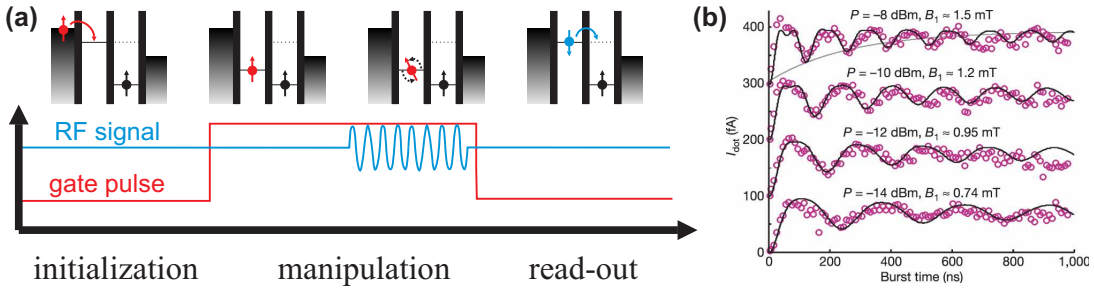

Fig. 9: *(a) Scheme of the pulse sequence for the manipulation and read-out in a double quantum dot. (b) Rabi oscillations observed experimentally (markers) and calculated (solid lines) for different magnetic fields B_1. The stronger the field, the faster is the spin rotation. Taken from ref. [13].*

CNOT gate is needed to form such a universal set. This was shown in ref. [14] and is discussed in more detail in the lecture "Fundamental Concepts of Quantum Information Processing" by T. Schäpers. On the other hand, as shown in ref. [1], the CNOT gate itself can be constructed from single spin rotations and the $\sqrt{SWAP}$ operation with

$$U_{CNOT} = e^{i(\pi/2)S_z^1} e^{-i(\pi/2)S_z^2} \sqrt{U_{SWAP}} e^{i(\pi)S_z^1} \sqrt{U_{SWAP}}. \tag{5}$$

Be aware that the operations have to be applied from right to left and that they do not necessarily commute. The single spin rotations of the two spins $i = 1, 2$ by an angle θ about the axis $a = x, y, z$ are realized by $e^{i(\theta)S_a^i}$, with the Pauli spin matrices S_a. The $SWAP$ operation exchanges the information between two qubits, i.e. $|\uparrow\downarrow\rangle$ is converted into $|\downarrow\uparrow\rangle$ while $|\uparrow\uparrow\rangle$ and $|\downarrow\downarrow\rangle$ do not change. With the basis

$$\begin{pmatrix} |\uparrow\uparrow\rangle \\ |\uparrow\downarrow\rangle \\ |\downarrow\uparrow\rangle \\ |\downarrow\downarrow\rangle \end{pmatrix} \widehat{=} \begin{pmatrix} |00\rangle \\ |01\rangle \\ |10\rangle \\ |11\rangle \end{pmatrix} \quad \text{and} \quad U_{SWAP} = \begin{pmatrix} 1 & 0 & 0 & 0 \\ 0 & 0 & 1 & 0 \\ 0 & 1 & 0 & 0 \\ 0 & 0 & 0 & 1 \end{pmatrix} \tag{6}$$

$$\sqrt{U_{SWAP}} = \begin{pmatrix} 1 & 0 & 0 & 0 \\ 0 & 0.5+0.5i & 0.5-0.5i & 0 \\ 0 & 0.5-0.5i & 0.5+0.5i & 0 \\ 0 & 0 & 0 & 1 \end{pmatrix}. \tag{7}$$

Starting in the product base, i. e. exchange coupling $J \to 0$, U_{SWAP} should exchange the spin information between the two qubits ($|\uparrow\downarrow\rangle \to |\downarrow\uparrow\rangle$). The product base can be expressed as coherent superposition of $|S\rangle$ and $|T_0\rangle$:

$$|\uparrow\downarrow\rangle = (|\uparrow\downarrow\rangle - |\downarrow\uparrow\rangle + |\uparrow\downarrow\rangle + |\downarrow\uparrow\rangle)/2 = (|S\rangle + |T_0\rangle)/\sqrt{2} \tag{8}$$

Now the exchange coupling J is switched on for a time t_{swap} and with

$$\int_0^{t_{swap}} J(t)/\hbar \, dt = \pi \tag{9}$$

equation (8) is transformed into

$$(|S\rangle + e^{-i\pi}|T_0\rangle)/\sqrt{2} = (|S\rangle - |T_0\rangle)/\sqrt{2} = (|\uparrow\downarrow\rangle - |\downarrow\uparrow\rangle - |\uparrow\downarrow\rangle - |\downarrow\uparrow\rangle)/2 = -|\downarrow\uparrow\rangle \quad (10)$$

This is the state that was supposed to be reached, and the exchange coupling is switched of again. Note that there the final state has the wrong sign, but this corresponds to a "global phase" factor ($\phi = \pi$), which can be ignored [15]. The beauty of this approach is that in order to implement a $\sqrt{SWAP}$, the exchange coupling is simply turned off after the time $t_{swap}/2$ [16]. This procedure has been successfully implemented by Petta et. al [17], and in the following we shall see how it has been done.

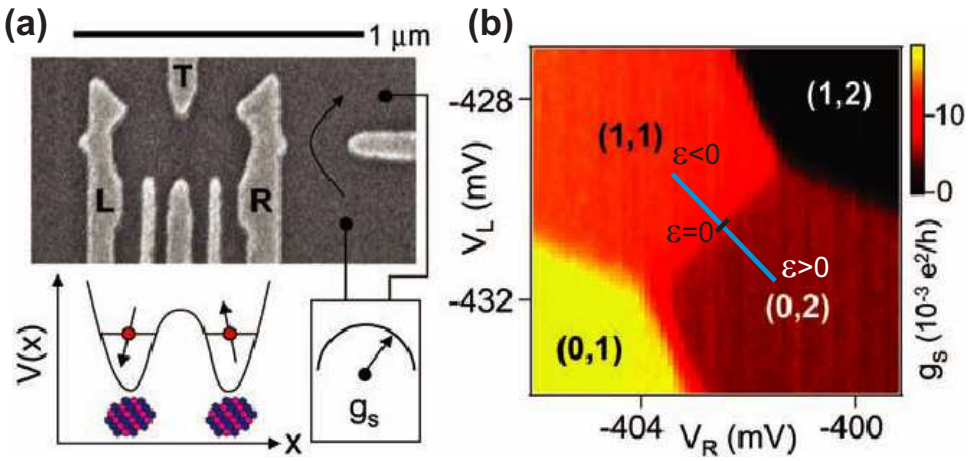

Fig. 10: *(a) Double quantum dot structure with a QPC next to the right gate. The state of the double quantum dot is detected by the current through the QPC (b). The occupation of the dot is denoted by (m,n), with m (n) the number of electrons in left (right) dot. It can be tuned by voltages V_L, V_R applied to the gates L and R. The figures are adapted from [17].*

Since a two qubit gate is to be done, a double quantum dot system as in Fig.10a has to be used. The occupation of the double dot is controlled by the voltages on the left (L) gate V_L and right (R) gate V_R, respectively, with the so-called "detuning" $\epsilon \propto (V_R - V_L)$. The gate T, which tunes the tunnel barrier between the two dots, is set to a value that gives a very weak the tunnel coupling. Therefore, the exchange interaction is very small ($J \to 0$) if the double dot is deep in the regime where each dot is occupied with one electron (1,1). A QPC next to the right dot serves as charge detector. It is tuned to be most sensitive in the regime, where either two electrons are in the right dot and the left dot is empty (0,2) for positive detuning, or where one electron occupies each dot (1,1) for negative detuning (see Fig.10b). The exchange coupling J is tuned with ϵ along the line in Fig.10b and is negligibly small for $\epsilon < -2$ mV.
Before the $SWAP$ operation can be done, the two qubit system has to be initialized in the $|\uparrow\downarrow\rangle$ state. This is done in three steps as depicted in Fig.11a-c. The system is prepared in the (0,2) singlet state $|S\rangle$ (Fig.11a). It cannot be in a $|T_0\rangle$, since this state is split off by the exchange coupling, which is large for positive detuning ϵ. Now, ϵ is changed to a negative value, thus separating the two electrons. They still form a singlet state, since they were in an eigenstate before. If there was no other interaction present, the electrons would remain in this state forever. However, besides the external magnetic field $B_0 = 100$ mT, which is the same for both quantum dots, a nuclear magnetic field B_N is present as well. This field mixes the $|S\rangle$ and the $|T_0\rangle$ state. This mixing is different for the two spins since B_N is different for the two

dots. Since they are no longer coupled to each other, the spins dephase on a time scale of about $\tau_{mix} \approx 20$ ns (Fig.11b) [17].

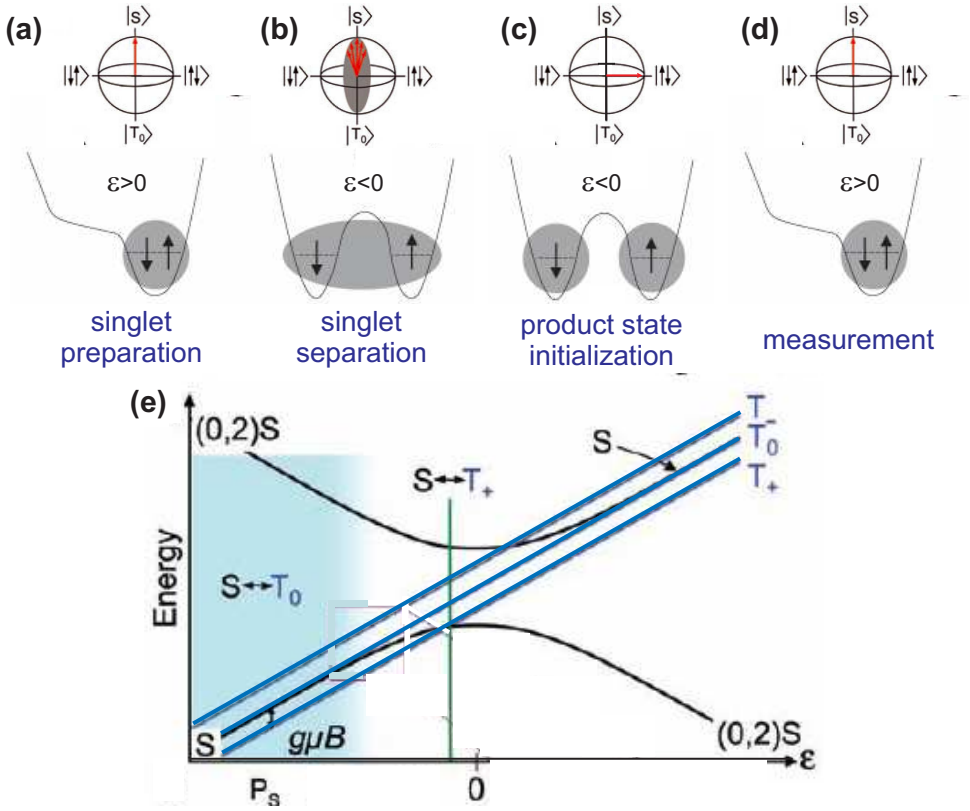

Fig. 11: *(a) Preparation of the double quantum dot in the (0,2) singlet state. (b) When the singlet is separated swiftly, the $|S\rangle$ state dephases. (c) If the separation is done slowly compared to the nuclear mixing time, the system is initialized in a product state. (d) The qubit state is measured by projection into the $|S\rangle$ - $|T_0\rangle$ base of the system. The (0,2) occupation can be reached only if the electrons form a singlet. The qubit state before the measurement can be deduced from the singlet probability. (e) Level scheme close to the (1,1)-to(0,2) transition depending on the detuning. For large negative detuning, the $|S\rangle$ and $|T_0\rangle$ states mix (blue background). At detuning of about $\epsilon \approx -1.2$ mV the $|T_0\rangle$ starts to split of from the $|S\rangle$ state due to finite exchange coupling. The $|S\rangle$ mixes with $|T_+\rangle$ at about $\epsilon \approx 0.5$ mV indicated by the green line. All triplet states are much higher in energy than the singlet (0,2). The figures are adapted from [17].*

If the transition towards negative detuning is done on a much larger timescale ($\tau_A \approx 1\,\mu$s) than this nuclear mixing time the spins still interact during the transition. This is called "adiabatic passage" and leads to a state with maximum mixing between $|S\rangle$ and $|T_0\rangle$ (both have the same probability amplitude). The phase is fixed and the spins form a product state as in eq. (8) and in Fig.11c. After some time the state is projected by tuning back to $\epsilon > 0$. If the state did not develop, it will be projected back to $|S\rangle$ Fig.11d. However, if it evolved to $|\downarrow\uparrow\rangle$ the system will now form a $|T_0\rangle$ state. Then the electron of the left dot cannot tunnel onto the right dot, because the $|T_0\rangle$ for the (0,2) configuration is too high in energy (Fig.11e).
The implementation of the $SWAP$ gate is shown in Fig.12a. The two outer Bloch spheres show the preparation and measurement of the spin states at positive detuning ϵ. Equations (8)-(10)

are represented by the three central Bloch spheres. In order to initialize the two qubit system in the $|\uparrow\downarrow\rangle$, ϵ is quickly tuned below -0.5 mV to prevent mixing between the $|S\rangle$ and $|T_+\rangle$ state due to the nuclear magnetic field (green lines in Fig.11e and 12a). Then ϵ is slowly ramped down further to provide the adiabatic passage necessary for the initialization.

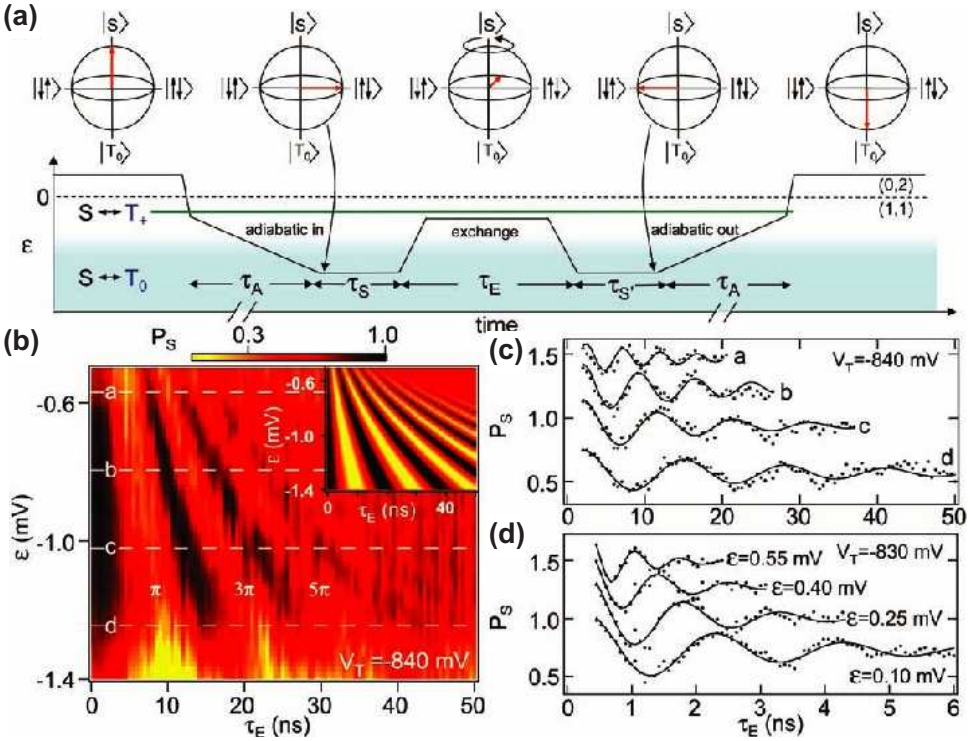

Fig. 12: *(a) Scheme for the $SWAP$ gate (b) Singlet probability P_S for different detunings during the exchange coupling and for different interaction times τ_E (c) Oscillations of the spin system during exchange coupling at different detuning marked as dashed lines in (b). (d) The oscillations are faster for weaker tunnel barrier (less negative voltage applied on gate T). The figures are adapted from [17].*

The detuning is then set to a level where the exchange coupling is larger or at least of the order of the nuclear field strength. Depending on ϵ and on the exchange time τ_E the system is rotated by an angle of $\theta = J(\epsilon)\tau_E/\hbar$. The angle of rotation θ is measured by the singlet probability (see Fig.12 b-d). A full $SWAP$ is applied for $\theta = \pi, 3\pi, 5\pi \ldots$ and the singlet probability reaches a minimum. The oscillations show that also rotations of $\theta = \frac{1}{2}\pi, \frac{3}{2}\pi, \frac{5}{2}\pi \ldots$ can be done which execute a $\sqrt{SWAP}$.
Combined with the single qubit rotations described in the previous section, a universal set of quantum gates is available for the quantum dot implementation of a quantum computer. Note that using ESR the single qubit phase gates in equation (5) cannot be carried out directly but have to be constructed form qubit rotations about the x-axis and y-axis [18].

5 Relaxation mechanisms

The fastest $\sqrt{SWAP}$ that could be done in [17] took $t = 180$ ps. This seems to be quite fast, but is it fast enough to fulfill the last DiVincenzo criterion on our list? The time it takes for a

gate has to be much shorter than the decoherence time T_2. In order to be able to apply error correction, at least 10^4 operations have to be done within T_2. The timescales and origins of spin relaxation in GaAs quantum dots will be discussed in this section.

5.1 Spin-energy relaxation

The flip of an exited spin state back to its ground state ($|\downarrow\rangle \rightarrow |\uparrow\rangle$) due to coupling with the phonon bath is called spin-energy relaxation or longitudinal relaxation and usually labeled T_1. For a spin qubit the result of such a process is a complete loss of information. It can be caused by modulation of the g-factor anisotropy due to vibrations of the crystal lattice or by relativistic coupling between the electron spin and the electric field of an emitted phonon. However, it turns out that the contributions of these direct processes to the spin energy relaxation are much smaller compared to the relaxation caused by the mixing of spin and orbital states due to spin-orbit (SO) interaction [19, 20].

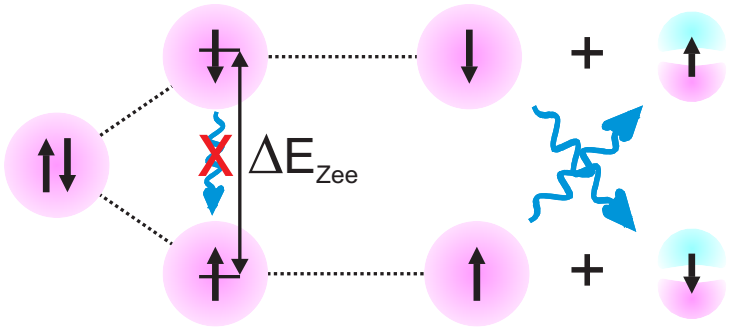

Fig. 13: *Without external magnetic field and in the absence of SO coupling, the spin states up and down are degenerate. They split by the Zeeman energy if a magnetic field is applied. Relaxation is not possible, because the direct contributions are very small and phonon coupling is prohibited. A small admixture of different spin and orbital states due to SO interaction allows phonon coupling.*

The SO Hamiltonian H_{SO} can be derived from the Dirac equation (see lecture "Electronic states in solids" by G. Bihlmayer). It consists of terms of the form $p_{x,y}\sigma_{x,y}$. Since the stationary states in a quantum dot are bound states with $\langle p_x\rangle = \langle p_y\rangle = 0$ due to the strong confinement in z, H_{SO} cannot couple different spin states of the same orbital d of the dot and

$$\langle d\downarrow|H_{SO}|d\uparrow\rangle \propto \langle d|p_x, y|d\rangle\langle\downarrow|\sigma_{x,y}|\uparrow\rangle = 0. \tag{11}$$

However, states that differ in both, the spin part as well as the orbital part, can be coupled [19]. If the Zeeman splitting is much smaller than the orbital splitting, the new eigenstates can be obtained from perturbation theory [21]

$$|d\uparrow\rangle^* = |d\uparrow\rangle + \sum_{d'\neq d} \frac{\langle d'\downarrow|H_{SO}|d\uparrow\rangle}{E_d - E_{d'} - \Delta E_{Zee}}|d'\downarrow\rangle \tag{12}$$

$$|d\downarrow\rangle^* = |d\downarrow\rangle + \sum_{d'\neq d} \frac{\langle d'\uparrow|H_{SO}|d\downarrow\rangle}{E_d - E_{d'} + \Delta E_{Zee}}|d'\uparrow\rangle \tag{13}$$

These new eigenstates (shown in Fig.13) can couple to electric fields. This leads to spin relaxation, but it also enables manipulation of the spin states by high frequency electric fields [22].
Relaxation between these new eigenstates can be of extrinsic origin, e.g., due to fluctuations of gate potentials or background charges. These and the influence of other noise sources can be kept small with a careful design of the device and turn out to be much less important compared to electric field fluctuations due to phonons. These can have two different origins. First, inhomogeneous deformations of the crystal lattice alter the band gap in space causing fluctuations of the electric field. Second, in polar crystals such as GaAs they can be caused by homogeneous strain due to the piezoelectric effect. It has been shown experimentally by studying spontaneous phonon emission that 2D and 3D piezoelectric phonons play an important role in GaAs double quantum dots [23].
The transition (relaxation) rate between the states $|d\downarrow\rangle^*$ and $|d\uparrow\rangle^*$ is given by Fermi's golden rule

$$\frac{1}{T_1} = \Gamma = \frac{2\pi}{\hbar}\sum_d |^*\langle d\uparrow|H_{e,ph}|d\downarrow\rangle^*|^2 D(\Delta E^*_{Zee}) \tag{14}$$

with the renormalized Zeeman splitting ΔE^*_{Zee}, the phonon density of states $D(E)$ at energy E and the electron-phonon coupling Hamiltonian $H_{e,ph}$ (ref. [21])

$$H^{\vec{q}j}_{e,ph} = M_{\vec{q}j} e^{i\vec{q}\vec{r}}(b^\dagger_{\vec{q}j} + b_{\vec{q}j}) \tag{15}$$

with electric field strength $M_{\vec{q}j}$ of phonon branch j (one longitudinal acoustic, two transversal acoustic) and with wave vector $\vec{q}$ at position $\vec{r}$ of the electron. $b^\dagger_{\vec{q}j}$ and $b_{\vec{q}j}$ are the phonon creation and annihilation operators. In the following we discuss the energy dependence of Γ and therefore the influence of an external magnetic field.
(i) First of all, we have to consider the phonon density of states in eq. (14). Spin-flip energies are much smaller than the energies of optical phonons and only (bulk) acoustic phonons are considered. Since they follow a linear dispersion relation, the phonon density of states increases quadratically with energy:

$$D(\Delta E_{Zee}) \propto \Delta E^2_{Zee} \tag{16}$$

(ii) The electric field strength of a phonon $M_{\vec{q}j}$ scales as $1/\sqrt{q}$ for piezoelectric phonons and as $\sqrt{q}$ for deformation potential phonons with wavenumber q. In GaAs, the effect of piezoelectric phonons dominates at energies below ≈ 0.6 meV [21]. At sufficiently small energies

$$M_{\vec{q}j} \propto 1/\sqrt{q} \propto 1/\sqrt{\Delta E_{Zee}} \tag{17}$$

Since (15) enters (14) quadratically, this adds as a factor of $1/\Delta E_{Zee}$.
(iii) Substituting eqs. (12), (13) and (15) into eq. (14), a matrix element $\langle d\uparrow|e^{i\vec{q}\vec{r}}|d'\uparrow\rangle$ is obtained describing how efficiently different orbitals are coupled by phonons. This matrix element vanishes for phonon wavelengths much shorter than the dot size l_{dot}, because the electron-phonon interaction is averaged out. The spin relaxation is fastest when the phonon wavelength is comparable to l_{dot}. For phonon wavelengths much larger than l_{dot}, the dot potential shifts uniformly up and down and different orbitals are no longer coupled efficiently. The phonon wavelength is hc_{ph}/E_{ph} and with the speed of sound in GaAs $c_{ph} \sim 4000$ m/s this yields a phonon wavelength $\lambda_{ph} \approx 16$ nm for a phonon energy $E_{ph} = 1$ meV. The Zeeman splitting and

therefore the phonon energy contributing to relaxation stays below $\Delta E_{Zee} < 200\,\mu$eV up to a magnetic field of $B_0 = 8$ T. Thus, $\lambda_{ph} \gg l_{dot}$ and the matrix element scales with

$$\langle d \uparrow |e^{i\vec{q}\vec{r}}| d' \uparrow \rangle \propto q \propto \Delta E_{Zee} \tag{18}$$

This enters eq. (14) quadratically, adding a factor of ΔE_{Zee}^2.
(iv) Without finite Zeeman splitting, the various terms obtained by expanding eq. (14) using eqs. (12) and (13) cancel out [20], which is known as "van Vleck"-cancellation. It is due to the fact that the spin-orbit interaction obeys time-reversal symmetry. The SO induced rotation during half a cycle of the electric field oscillation is reversed in the second half. Thus, no net rotation takes place. Applying an external field B_0 breaks the time-reversal symmetry, because the SO interaction is of the same direction as B_0 for one half of the cycle, while it is opposite for the other half. This leads to a B_0^2 dependence of the relaxation rate [20] and

$$\Gamma_{Zee} \propto \Delta E_{Zee}^2. \tag{19}$$

Taking the contributions of eqs. (16), (17), (18) and (19) together with (15) and (14), the relaxation rate $1/T_1$ is proportional to B_0^5 since $\Gamma \propto \Delta E_{Zee}^2 \cdot \Delta E_{Zee}^{-1} \cdot \Delta E_{Zee}^2 \cdot \Delta E_{Zee}^2 = \Delta E_{Zee}^5$. For temperatures $T \gg g\mu_B B_0/k_B$ the finite phonon occupation N_{ph} leads to stimulated emission. It is accounted for by multiplying (14) with a factor $1 + N_{ph}$. The phonon occupation is given by the Bose-Einstein distribution. Therefore, $N_{ph} \propto k_B T/\Delta E_{Zee}$, and the relaxation rate is expected to follow a B_0^4 dependence. This has been observed experimentally in [24] where relaxation times up to $T_1 = 1$ s have been observed as shown in Fig.14. The same publication demonstrates the influence of the confinement on the SO interaction and thus on the relaxation time by changing the size of the quantum dot.

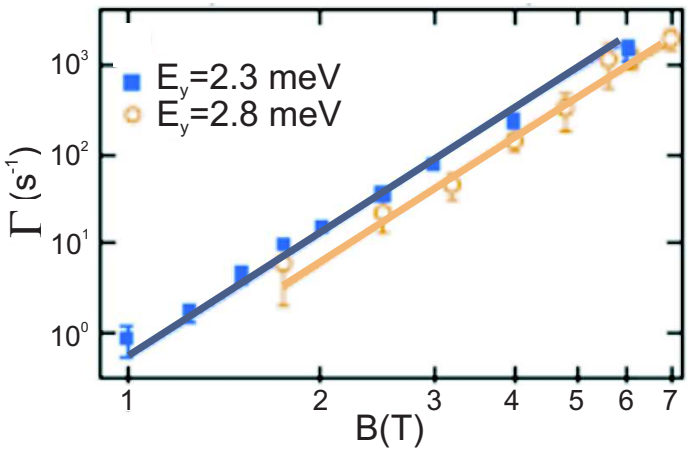

Fig. 14: *Spin-energy relaxation rates for two different confinement potentials. The markers are data points, the solid lines a fit with theory showing the expected B_0^4 dependence. The data set for weaker confinement (yellow) and thus smaller SO interaction shows smaller rates. Adapted from ref. [24].*

Besides the SO coupling there is another mechanism leading to spin-energy relaxation. Near zero field the electron spins and nuclear spins can flip-flop due to the hyperfine interaction. The electron spin evolves about the nuclear field but the nuclei also evolve around the electron spin. The field experienced by the nuclei leads to a shift of their resonance frequencies in nuclear magnetic resonance (NMR), the so-called Knight shift [25]. Since it is averaged over many

nuclei it can be taken as scalar and its strength is $A_k \approx 10\,\mu\text{s}^{-1}$ [21]. The Hamiltonian of the hyperfine interaction is

$$H_{HF} = \sum_k^N I_k \overleftrightarrow{A_k} S = \sum_k^N A_k I_k S = \sum_k^N A_k (I_k^+ S^- + I_k^- S^+ 2 I_k^z S_z)/2 \tag{20}$$

for N nuclei in the quantum dot, with $S^\pm$ and $I^\pm$ the raising and lowering operators of the electron spin and the nuclear spin, respectively. Typically, $N \approx 10^6$ in a GaAs lateral quantum dot. This leads to electron nuclear spin flip-flops and thus electron spin relaxation on a timescale of $10\,\mu$s. The energy difference between nuclear spins and electron spins grows rapidly with B_0 and flip-flops are prohibited. The SO interaction remains as the only active spin-energy relaxation mechanism at high magnetic fields.

5.2 Dephasing and decoherence

The spin-energy relaxation is due to SO coupling alone for $B_0 > 0$. If this were true as well for the phase relaxation or decoherence time T_2 (also called "transversal" spin relaxation), then we would have $T_2 = 2T_1$ [26]. Unfortunately, this is not the case. Phase relaxation does not necessarily depend on energy and fluctuations of the nuclear spins lead to decoherence of the electron spin via the hyperfine coupling. In the following we will analyze this process in more detail.

Electron spins experience a magnetic field due to the hyperfine coupling, which is called the Overhauser field. With eq. (20) and $(\sum_k^N A_k \vec{I}_k)\vec{S} = g\mu_B \vec{B}_N \vec{S}$ it is

$$\vec{B}_N = \sum_k^N A_k \vec{I}_k / g\mu_B \tag{21}$$

and of random, unknown value. Thus, the electron spin evolves in an unknown way. For fully polarized nuclear spins $B_{N,\text{max}} = 5$ T in GaAs [27]. Under experimental conditions only a small average polarization with Boltzmann statistics adds to the external field. Statistical fluctuations of the $N \approx 10^6$ nuclei of the quantum dot around this average, for spin $1/2$ similar to N coin tosses, lead to a root mean square value of the magnetic field of $B_{rms} = B_{N,\text{max}}/\sqrt{N} \approx 5$ mT, which has been confirmed experimentally [28].

The electron spin precesses about a magnetic field given by $\vec{B}_{tot} = \vec{B}_0 + \vec{B}_N$. The z-component of $\vec{B}_N$ changes the precession frequency. For $B_N^z = 1$ mT the precession rate is increased by $\Delta\nu = g\mu_B B_N^z/h = 6$ MHz and the electron spin picks up an extra phase of $180°$ within 83 ns [21]. The influence of the other components $B_N^{x,y}$ depends on their strength compared to B_0. The precession axis will be close to the x,y-plane for $B_N^{x,y} \gg B_0$. In an experiment typical values are $B_0 = 1$ T and $B_N^x \sim 1$ mT and thus, $B_N^{x,y} \ll B_0$. The precession frequency changes by $\Delta\nu \approx g\mu_B B_N^2/2B_0 = 3$ kHz causing an extra phase of $180°$ after 166 ms. The precession axis is changed by $arctan\,(B_N/B_0)$ and therefore tilted by $\approx 0.06°$. In most of the experiments $B_0 \geq 100$ mT and only B_N^z is of relevance.

If B_N^z were constant and known, its influence would not be a source of decoherence. However, B_N is fluctuating, for instance due to dynamic nuclear polarization or flip-flops of two nuclear spins with different hyperfine coupling A_k. The electron spin will pick up a random phase depending on the value of the nuclear field. For a nuclear field that is randomly drawn from a Gaussian distribution of nuclear fields with the standard deviation of $\sigma = \sqrt{\langle (B_N^z)^2 \rangle}$ (see Fig.15a), the decay of the coherence will take the form $\exp\left[-t^2/(T_2^*)^2\right]$ with (after ref. [29])

$$T_2^* = \frac{\hbar\sqrt{2}}{g\mu_B\sqrt{\langle (B_N^z)^2\rangle}} \quad . \tag{22}$$

The dephasing time T_2^* will be 37 ns for a nuclear field of $B_N^z = 1$ mT. In the experiment reported in ref. [17] and shown schematically in Fig.15b, $T_2^* = 10$ ns has been measured for the dephasing between a separated $|S\rangle$ and a $|T_0\rangle$ state corresponding to a field of $B_N^z = 2.3$ mT. Note that the dephasing time T_2^* can be much shorter than the decoherence time T_2. The effect of the nuclear field can be compensated if it assumes an unknown but constant value during the experiment, i.e. if the timescale of the fluctuations is very long compared to the timescale of the experiment (see p. 5.2).

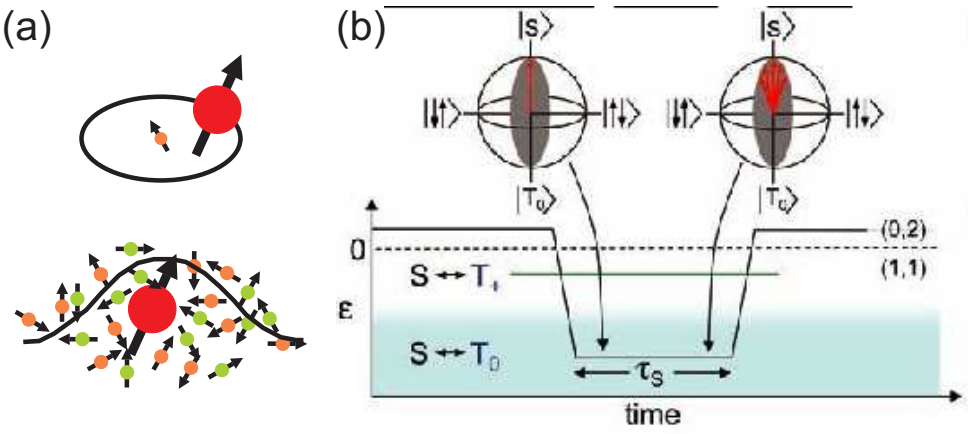

Fig. 15: *(a) One electron interacts with a single nuclear spin (top) or many nuclear spins with a Gaussian field distribution (bottom). (b) Dephasing between a separated $|S\rangle$ and a $|T_0\rangle$ state due to different random value of B_N^z at the site of each electron. Taken from ref. [17].*

The timescales of the nuclear field fluctuations depend on the interactions of the nuclei. The two most important mechanisms in this respect are the electron-nuclear hyperfine interaction [30] and the magnetic dipole interaction between the nuclei [31]. The first we already discussed in connection with the spin-energy relaxation of the electrons. Eq. (20) is only effective at $B_0 = 0$ for the electron spins. It is also most effective for nuclear spins under this condition. But the hyperfine interaction can affect B_N^z indirectly via virtual nuclear electron flip-flops between one nucleus and the electron and the electron and another nucleus. This does not affect the electron spin but leads to a flip-flop between two nuclei m and n, which changes B_N^z if $A_m \neq A_n$. As discussed in section 5.1 for the electrons, the nuclei change on a $10\,\mu$s timescale due to the Knight shift. At large magnetic fields B_0 this process will be suppressed.
In a strong external magnetic field, only the secular part of the magnetic dipole interaction Hamiltonian H_D has to be considered and

$$H_D \propto \vec{I}_m \cdot \vec{I}_n - 3I_m^z I_n^z = I_m^x I_n^x + I_m^y I_n^y - 2I_m^z I_n^z = (I_m^+ I_n^- + I_m^- I_n^+ - 4I_m^z I_n^z)/2 \quad . \tag{23}$$

The terms with the nuclear spin ladder operators $I^\pm$ vanish for coupling between different isotopes at high fields. Since the effective magnetic dipole interaction between neighboring nuclei in GaAs is about $(100\,\mu\text{s}^{-1})$ [32], $B_N^{x,y}$ change on the same timescale given by $I_m^z I_n^z$ in eq. (23). The flip-flop terms affect B_N^z but they can be strongly suppressed if $|A_m - A_n|$ is larger than

the coupling between two nuclei. Thus, B_N^z may evolve more slowly compared to the $100\,\mu$s timescale for the dipolar interaction alone.
All in all, the relevant interactions lead to moderate time scales of $t_{\rm nuc} = 10 - 100\,\mu$s for the fluctuations of the nuclear magnetic field B_N. At high B_0, the timescale for fluctuations of B_N^z is expected to be much longer. However, this has not yet been confirmed experimentally.
For spin evolution times smaller than $t_{\rm nuc}$, the influence of the fluctuations can be refocused in a Hahn echo experiment as shown in Fig.16. After a dephasing time τ_S, a rotation by $\theta = J(\epsilon)\tau_E/\hbar = \pi$ around the z-axis of the Bloch sphere is carried out. Then the spins keep evolving in the same direction as they did before the π-pulse, so that now they evolve back towards $|S\rangle$. They reach their starting state after $\tau_{S'} = \tau_S$. If there is a loss of signal, it is due to random fluctuations during $\tau_{S'} + \tau_S + \tau_E$. The spin coherence in such an experiment T_{echo} decays with $\exp(-t^3/t_{\rm nuc}T_2^{*2})$ [33]. Taking $T_2^* = 10$ ns and $t_{\rm nuc} = 10\,\mu$s, this leads to $T_{echo} = 1\,\mu$s. This is indeed the timescale obtained from the experiment in Fig.16.

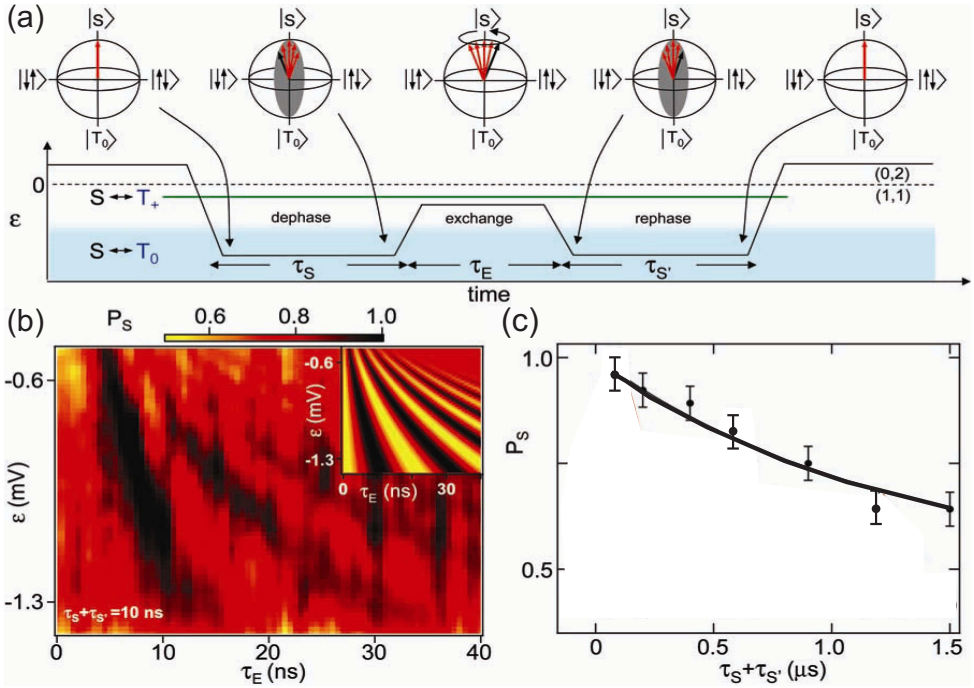

Fig. 16: *(a) The Hahn echo pulse sequence as described in the text. All transistions are done with rapid adiabatic passage so that the qubit stays all the time in the singlet-triplet base and does not change to the product base. (b) Singlet probability P_S as a function of detuning and interaction time τ_E at fixed dephasing and rephasing time. The rotation angle around the z-axis leads to an oscillation of P_S with $\theta = J(\epsilon)\tau_E/\hbar$. (c) Decay of the echo amplitude. All figures adapted from ref. [17].*

6 Summary and outlook

In this lecture we have given an introduction to quantum computing with electron spins in semiconductor quantum dots as qubits. We have shown that the qubit state can be measured with an accuracy up to 81%. Single qubit rotations can be carried out using ESR locally coupled to the quantum dot. Two qubit gates can be performed by tuning the exchange interaction between

two electrons in neighboring quantum dots. In particular, the $\sqrt{SWAP}$ operation has been introduced as a universal quantum gate. Last but not least, the origins and timescales of spin-energy relaxation and spin decoherence were discussed. The spin-energy relaxation time can be as long as $T_1 = 1$ s, depending strongly on the magnetic field B_0 and on the spin-orbit interaction. Decoherence occurs due to fluctuations of the nuclear magnetic field. Its lower bound is found so far to be $T_2 \approx 1.2\,\mu$s. Within this time, a fast $\sqrt{SWAP}$ of $180ps$ can be carried out almost 7000 times. Thus, the decoherence time seems to be sufficiently long and all DiVincenzo criteria are fulfilled.

Why then do we not already have a quantum computer? First of all, the universal gate is the $CNOT$ and composed of two $\sqrt{SWAP}$ and three single spin rotations (see eq. 5). With today's technique the latter alone take about 600 ns. They could be performed faster using a stronger B_1 field for the manipulation. However, this also increases the coupling of the electric field eventually masking the ESR effect. Materials with a larger g-factor would provide better coupling to the magnetic field and for $g \sim 2$ also the SO interaction would be small. The latter would improve the spin-energy relaxation time as well. The dephasing time itself should increase significantly in materials with less or without nuclear spins. Currently investigated as alternatives which could provide these properties are for instance quantum dots in SiGe 2DEGs or in carbon nanotubes.

Compared to the yet too short decoherence time, other limitations seem to be minor challenges. The visibility of the read-out still needs to be improved and also a gate geometry which would be scalable to hundreds or thousands of qubits needs to be developed. Although the semiconductor quantum dots remain a promising implementation for a solid state quantum computer, still a lot of work is to be done.

References

[1] D. Loss, D. P. DiVincenzo, Phys. Ref. A **57**, 120 (1998)

[2] C. Monrow, D. M. Meekhof, B. E. King, W. M. Itano, D. J. Wineland, Phys. Rev. Lett. **75**, 4714 (1995)

[3] A. Shnirman, G. Schön, Z. Hermon, Phys. Rev. Lett. **79**, 2371 (1997)

[4] B. E. Kane, Nature **393**, 133 (1998)

[5] B. van Wees, L. P. Kouwenhoven, E. M. M. Willems, C. J. P. M. Harmans, et al., Phys. Ref. B **43**, 12431 (1991)

[6] M. Field, C. G. Smith, M. Pepper, D. A. Ritchie, J. E. F. Frost, G. A. C. Jones, D. G. Hasko, Phys. Rev. Lett. **70**, 1311 (1993)

[7] J. M. Elzerman, R. Hanson, J. S. Greidanus, L. H. Willems van Beveren et al., Phys. Rev. B **67**, 161308 (2003)

[8] A. C. Johnson, J. R. Petta, C. M. Marcus, M. P. Hanson, A. C. Gossard, Phys. Rev. B **72**, 165308 (2005)

[9] L. M. K. Vandersypen, J. M. Elzerman, R. N. Schouten, L. H. Willems van Beveren et al., Appl. Phys. Lett. **85**, 4394 (2004)

[10] J. M. Elzerman, R. Hanson, L. H. Willems van Beveren, B. Witkamp et al., Nature **430**, 431 (2004)

[11] R. Hanson, L. H. Willems van Beveren, I. T. Vink, J. M. Elzerman et al., Phys. Rev. Lett. **94**, 196802 (2005)

[12] C. P. Slichter, *Principles of Magnetic Resonance* (Springer, Berlin, 1990)

[13] F. H. L. Koppens, C. Buizert, K. J. Tielrooij, I. T. Vink et al., Nature **442** , 766 (2006)

[14] A. Barenco et al., Phys. Rev. A **52**, 3457 (1995)

[15] M. A. Nielsen, I. L. Chuang, *Quantum Computation and Quantum Information* (Cambridge University Press, Cambridge, 2000)

[16] V. Cerletti, W. A. Coish, O. Gywat, D. Loss, Nanotechnology **16**, R27 (2005)

[17] J. R. Petta, A. C. Johnson, J. M. Taylor, E. A. Laird et al., Science **309**, 2180 (2005)

[18] J. Stolze, D. Suter, *Quantum Computing* (Wiley-VCH, Berlin, 2004)

[19] A. V. Khaetskii, Yu. V. Nazarov, Phys. Rev. B **61**, 12639 (2000)

[20] A. V. Khaetskii, Yu. V. Nazarov, Phys. Rev. B **64**, 125316 (2001)

[21] R. Hanson, L. P. Kouwenhoven, J. R. Petta, S. Tarucha, L. M. K. Vandersypen, Rev. Mod. Phys. **79**, 1217 (2007)

[22] K. C. Nowack, F. H. L. Koppens, Yu. V. Nazarov, L. M. K. Vandersypen, Science **318**, 1430 (2007)

[23] T. Fujisawa, T. H. Oosterkamp,W. G. van der Wiel, B. W. Broer et al., Science **282**, 932 (1998)

[24] S. Amasha, K. MacLean, I. Radu, D. M. Zumbühl et al., Phys. Rev. Lett. **100**, 046803 (2008)

[25] W. D. Knight, Phys. Rev. **76**, 1259 (1949)

[26] V. N. Golovach, A. Khaetskii, D. Loss, Phys. Rev. Lett. **93**, 016601 (2004)

[27] D. Paget, G. Lampel, B. Sapoval, V. I. Safarov, Phys. Rev. B **15**, 5780 (1977)

[28] F. H. L. Koppens, J. A. Folk, J. M. Elzerman, R. Hanson et al., Science **309**, 1346 (2005)

[29] I. A. Merkulov, Al. L. Efros, M. Rosen, Phys. Rev. B **65**, 205309 (2002)

[30] A. V. Khaetskii, D. Loss, L. Glazman, Phys. Rev. Lett. **88**, 186802 (2002)

[31] R. de Sousa, S. Das Sarma, Phys. Rev. B **67**, 033301 (2003)

[32] R. G. Shulman, B. J. Wyluda, H. J. Hrostowski, Phys. Rev. **109**, 808 (1958)

[33] B. Herzog, E. L. Hahn, Phys. Rev. **103**, 148 (1956)